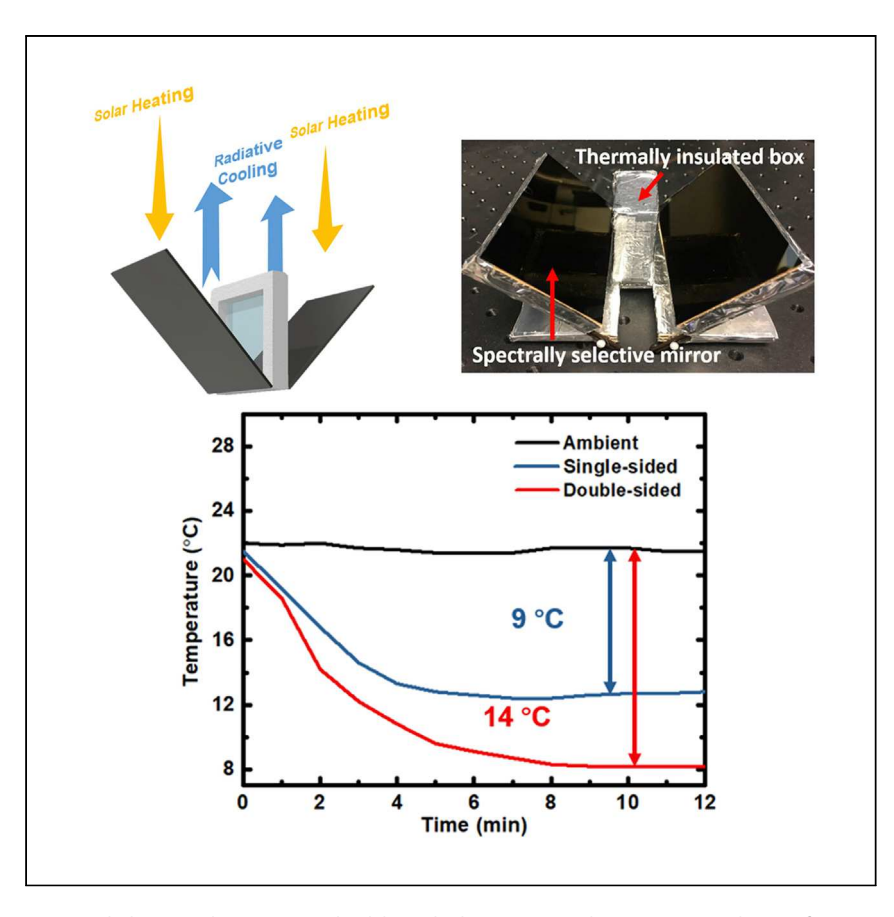




Article

Hybrid concentrated radiative cooling and solar heating in a single system



Gan and Zhou et al. present a double-sided passive cooling system with significant cooling performance that requires no consumption of electricity. By directing thermal emission from both surfaces of a vertically aligned emitter to the sky, they realize a temperature reduction of over 12° C in an outdoor environment.

Lyu Zhou, Haomin Song, Nan Zhang, ..., Boon S. Ooi, Zongfu Yu, Qiaoqiang Gan

qqgan@buffalo.edu

HIGHLIGHTS

A double-sided architecture couples thermal radiation from both sides of the emitter

A system capable of simultaneously performing radiative cooling and solar heating

Temperature reduction of 14.5°C obtained under laboratory conditions

Over 12°C temperature reduction obtained in an outdoor environment

Zhou et al., Cell Reports Physical Science $\it 2$, 100338

February 24, 2021 © 2021 The Author(s). https://doi.org/10.1016/j.xcrp.2021.100338



Article

Hybrid concentrated radiative cooling and solar heating in a single system

Lyu Zhou,^{1,4} Haomin Song,^{1,4} Nan Zhang,¹ Jacob Rada,¹ Matthew Singer,¹ Huafan Zhang,² Boon S. Ooi,² Zongfu Yu,³ and Qiaoqiang Gan^{1,5,*}

SUMMARY

Radiative cooling is an emerging sustainable technology that does not require electricity to function. However, to realize sub-ambient cooling, the effects of the undesired incident solar energy must be minimized. Considering an ideal blackbody radiator at 300 K, the maximum cooling power density is $\sim\!160~\text{W/m}^2$. Here, we report an architecture capable of overcoming this challenge by using two spectrally selective mirrors to simultaneously absorb the incident sunlight and re-direct the thermal emission from a vertically aligned emitter. With this configuration, both sides of the vertical emitter can be used together to realize a measured local cooling power density of over 270 W/m^2 in a controlled laboratory environment. Under standard atmospheric pressure, we realized cooling that was 14°C below the ambient temperature in the laboratory environment and a more than 12°C temperature reduction in outdoor testing.

INTRODUCTION

Electricity-driven cooling is one of the major end uses of energy that is responsible for global peak electricity demand. For instance, the global annual energy consumption for cooling buildings is \sim 1,260 TWh/year. Of the fuel used in vehicles (e.g., 13 million barrels of oil equivalent per day in 2012²), \sim 29% is used for cooling, and 25%–33% is lost because of heat dissipation. Therefore, passive cooling that cools without electricity or fuel could significantly affect global energy consumption.

Because of the transparency of the Earth's atmosphere within a wavelength range of $8-13 \mu m$, objects can passively realize a cooling effect by emitting their heat within this spectral window. Building on this heat exchange channel, sky cooling emerges as an electricity-free cooling technology. However, there are two major challenges that must be addressed to implement this electricity-free cooling technology in a practical environment: (1) the object has to have direct access to the sky (i.e., with direct sky-facing emitting surfaces), and (2) the material/structure must have minimal solar light absorption while also strongly emitting thermal radiation between 8-13 μm for day-time cooling. In recent years, many groups have attempted to discover radiative cooling effects in biomaterials^{5,6} and develop high-performance and low-cost thermally emissive metamaterials. 7-14 Various advanced thermal photonic materials and systems with different spectral selection features have been reported, mainly focusing on blocking 14,15 or scattering the incident sunlight to suppress its heating effect. 8,12,13,16 The average measured cooling power densities of these devices are $\sim 100 \text{ W/m}^2$ during the day and $\sim 120 \text{ W/m}^2$ during the night. ^{17–20} However, considering the blackbody radiation limit at ambient temperature (e.g., at 300 K), the maximum cooling power density for a sky-facing radiative cooling device

¹Department of Electrical Engineering, The State University of New York at Buffalo, Buffalo, NY 14260, USA

²KAUST Nanophotonics Lab, King Abdullah University of Science and Technology, Thuwal 23955-6900, Saudi Arabia

³Department of Electrical and Computer Engineering, University of Wisconsin, Madison, WI 53705, USA

⁴These authors contributed equally

⁵Lead contact

^{*}Correspondence: qqgan@buffalo.edu https://doi.org/10.1016/j.xcrp.2021.100338



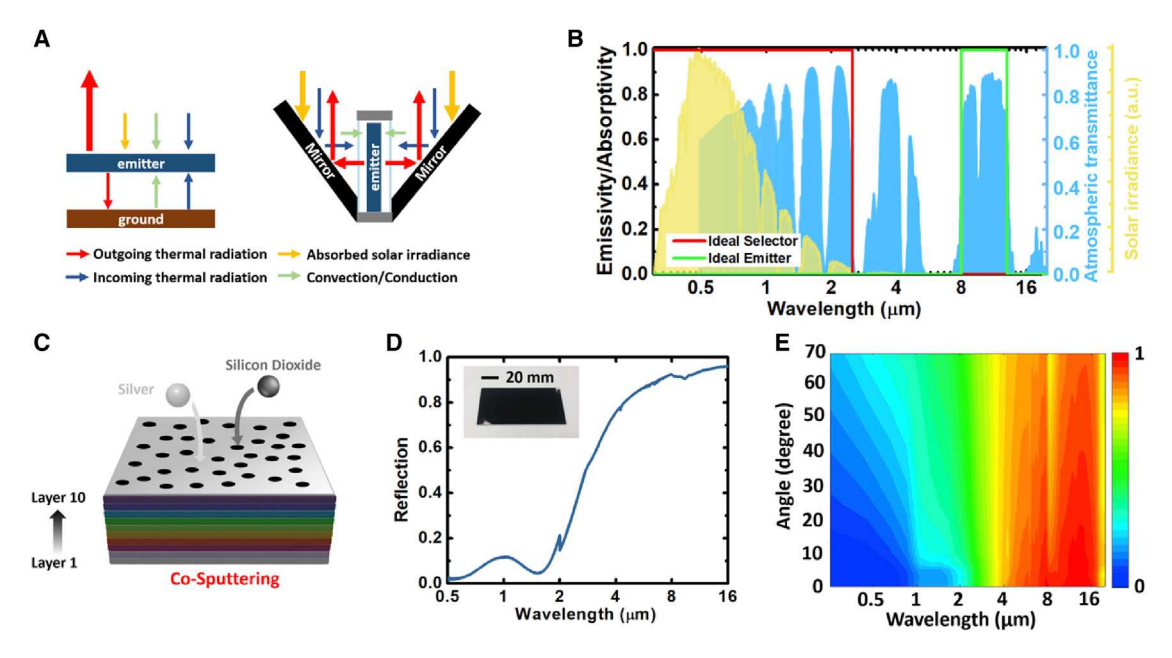


Figure 1. Design of the double-sided architecture for concentrated radiative cooling

(A) Diagrams of the power tradeoff in a conventional single-sided radiative cooling system (left panel) and a double-sided system (right panel), respectively. The red arrow indicates the outgoing thermal radiation from the emitter, the blue arrow indicates the incoming thermal radiation from the atmosphere and surrounding objects, the green arrow indicates the non-radiative power exchange, and the yellow arrow indicates the absorbed solar irradiation.

- (B) Emissivity of the ideal cases. The red line indicates an ideal selector and the green line indicates an ideal emitter for the daytime radiative cooling design. The AM 1.5 solar spectrum (yellow) and atmospheric transmittance (blue) are plotted for reference.
- (C) Schematic of the cermet-based solar spectral selector. Ten layers of Ag-SiO₂ nanocomposite were deposited with different mixture ratios.
- (D) The measured reflection spectrum of the solar spectral selector. The inset shows a photograph of a cermet-based solar-selective plate.
- (E) Measured angle-dependent reflection spectra of the solar-selective plate.

is \sim 160 W/m² (see calculation details in Note S1), 21,22 which is much less than the incident solar energy of \sim 1,000 W/m². Therefore, the overall effect on sustainability for radiative cooling technology would be questioned if this solar energy is sacrificed. ²³ It is therefore a great challenge for the recently developed, highly scattering thermal emitter materials to realize their maximum potential (i.e., to realize a peak cooling power of 160W/ m² or utilize a larger portion of the 1,000 W/m² of incident solar radiation) because these materials currently cannot do both. Here we report a double-sided architecture using two solar spectrally selective mirrors to redirect the thermal emission from a vertically aligned emitter and demonstrate a concentrated radiative cooling concept. Importantly, because of the spectral selectivity of the solar absorption mirror, this strategy did not waste the solar input energy. Instead, it is able to integrate the solar heating and radiative cooling effects within a single system with no need of extra spaces. By retaining a portion of the 1,000 W/m² of incident sunlight, the energy efficiency of the radiative cooling system as a whole can be improved greatly.

RESULTS AND DISCUSSION

A double-sided architecture

For a planar thin film thermal emitter, the top and bottom surfaces emit thermal radiation. However, only the sky-facing surface causes a noticeable cooling effect, as reported in previous radiative cooling experiments. ^{4–16,21–38} The bottom surface can only exchange thermal radiation with the ground (Figure 1A, left panel). Therefore, a waveguide strategy that can guide the thermal emission from the two surfaces to the

Article



sky will break the cooling power density limit of the single-sided thermal emitter. In this work, we report a double-sided architecture (with a vertical radiator) using a cermet-based solar spectral selector for concentrated radiative cooling.³⁹ This solar selector will function as a thermal radiation waveguide/mirror as well as a solar absorber (it is capable of absorbing over 90% of electromagnetic radiation within the solar spectrum while also maintaining a reflection of over 90% in the mid-infrared region, including 8-13 μm). When a vertical thermal radiator is coupled with this spectral selector (Figure 1A, right panel), its thermal emission can be mostly reflected to the sky while the incident solar energy is absorbed by the thermal selector. Both sides of a planar thermal emitter can be used to emit heat, and we realize a record-high local cooling power density of 273.3 W/m² in a laboratory environment, twice as much as the previously reported cooling power density of single sky-facing surfaces (i.e., a horizontal radiator). Without special vacuum thermal isolation, we realized a temperature reduction of 14°C below the ambient temperature in a laboratory environment and over 12°C in an outdoor test under standard atmospheric pressure. In addition, the spectral selectivity of the cermet-based plates enables efficient solar absorption and restrains thermal radiation, resulting in a tremendous temperature rise in the solar absorption plates. This simultaneous solar heating and radiative cooling configuration paves the way for wider application in hybrid solar heating and radiative cooling utilities (e.g., enabling integration of a thermoelectric generator into the same system).³⁸

In principle, to realize daytime radiative cooling, the emitter is required to be strongly absorptive in the mid-infrared wavelength range while minimizing absorption in the solar wavelength range (up to 2.5 μm, as shown in Figure 1B). Here we first employ a cermet-based solar spectral selector to realize this spectral selectivity. This type of material was initially created for solar heating applications with optimized spectral selectivity. 39,40 In our system, it efficiently absorbs solar light and simultaneously reflects thermal radiation from the emitter (as shown by the red curve in Figure 1B). In this experiment, 10 layers of co-sputtered Ag-SiO₂ nanocomposite films were stacked to construct the solar absorption film on a glass substrate, labeled layer 1 to layer 10 in Figure 1C (see fabrication details under Experimental procedures)^{41–46}. As a result, a strong spectrally selective solar absorber was realized. As shown in the inset in Figure 1D, the resulting film is visibly black. Its average reflectivity from visible to infrared (IR) (up to 2 μm) is below 8%. Intriguingly, its reflection increases rapidly and remains over 90% throughout the mid-infrared (MIR) spectral range, covering an atmospheric window of 8-13 µm (see its infrared image in Figure S1). Remarkably, this superior spectral selectivity can be retained over a broad incident angle range, as shown in Figure 1E; within the incident angle ranging between 0°-50°, the absorption remains over 90% in the solar spectral region while also maintaining a reflection of over 95% between 8–13 μm. More microscopic characterization results of the graded cermet-based solar absorption material are shown in Figure S2. In this work, we demonstrate an application of this solar heating material for hybrid concentrated radiative cooling and solar heating.

Indoor tests

As shown in Figure 2A, we built a V-shaped mirror structure with a thin-film thermal emitter in a polystyrene box with two open sides exposed to two solar absorption mirrors (at a tilt angle of 45°). The box was then sealed with a polyethylene film. As a result, thermal radiation from both sides of the emitter was directed to the remote heat sink (i.e., the sky or a black absorber at 77 K in this indoor test). Although this type of tilted mirror architecture has been shown in previous studies to improve the directionality of the thermal emission, ^{14,36} because of the spectrally selective



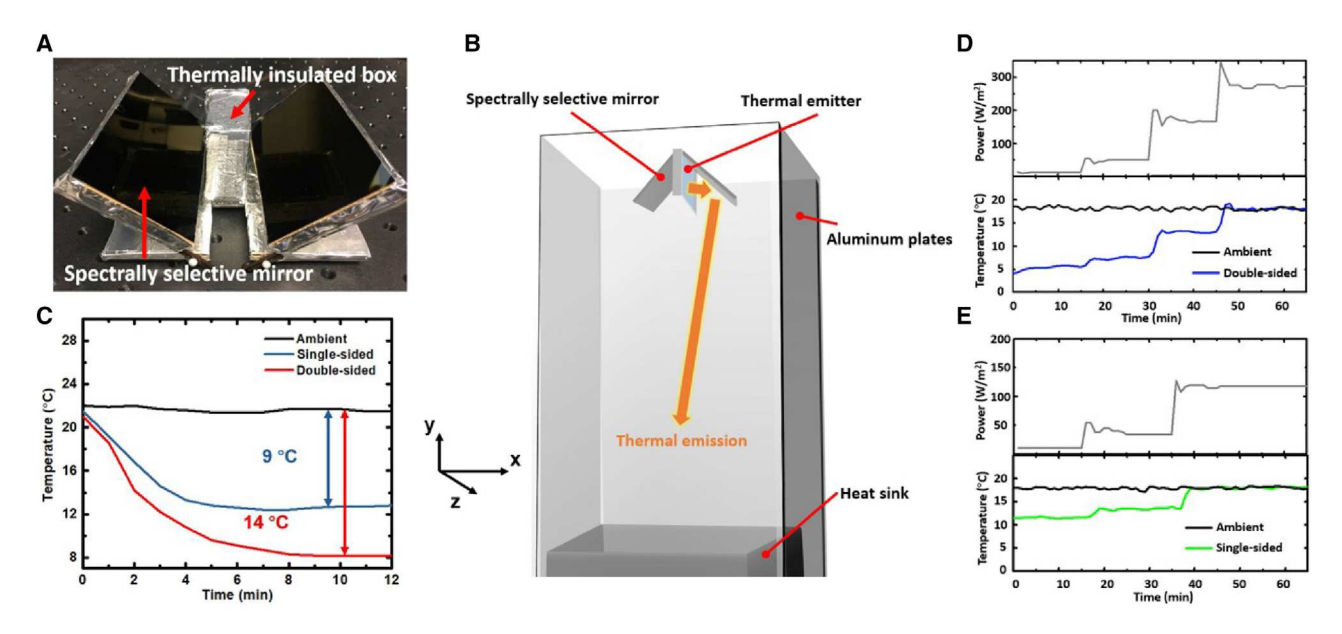


Figure 2. Radiative cooling performance of the double-sided thermal emitter system

- (A) A photo of the double-sided system made of a thermally insulated box with V-shape solar spectrally selective plates.
- (B) Schematic diagram of the indoor experimental setup.
- (C) Temperature measurements of the single-sided system (blue curve) and the double-sided system (red curve) in the laboratory environment. The black line shows the ambient temperature.

(D and E) Measured heater power and temperatures of the emitter in the (D) double-sided system and (E) single-sided system. The black, blue, and green curves indicate the ambient temperature and the temperature of the emitter in a double-sided system and a single-sided system, respectively. The measured heater powers (gray curves) in the top panels reveal the cooling powers of the double-sided and single-sided systems, respectively.

property of the mirror, this V-shaped configuration can direct thermal radiation from both sides of a standing planar emitter, achieving a record-breaking radiative cooling power density. To validate this hypothesis, we performed several proof-of-concept tests in a lab environment.

First, black aluminum foil immersed in liquid nitrogen was employed as a heat sink for the indoor radiative cooling test (similar to our previous work; 14 see Figure S3 for the emissivity spectrum of the black aluminum foil and other details regarding this indoor test under Experimental procedures). As shown in Figure 2B, the heat sink was connected to the tested device using an infrared-reflective aluminum plate waveguide. For this experiment, black aluminum was also used as the thermal emitter because of its near-unity emissivity over the IR spectrum range. As shown in Figure 2C, the measured air temperature around the emitter was \sim 22°C. As a result, the temperature of the double-sided system was reduced by $14^{\circ}C$ \pm 0.2° C, \sim 5°C lower than the control single-sided system (i.e., 9°C \pm 0.4°C). To experimentally reveal the cooling power density, we utilized a heat patch that was sandwiched between the black aluminum foil emitters to heat them to ambient temperature (following a procedure reported previously¹⁵). As shown in Figures 2D and 2E, the surface temperatures of the black aluminum in the double-sided system (with a vertical radiator) and the single-sided system (with a horizontal radiator) were plotted by blue (Figure 2D) and green (Figure 2E) curves, respectively. When they reached ambient temperature (i.e., the black curves with an average temperature of 18°C during these two experiments), the measured local cooling power densities were $273.3 \pm 4.0 \,\mathrm{W/m^2}$ for the double-sided system and $118.6 \pm 0.5 \,\mathrm{W/m^2}$ for the single-sided system (see gray curves in Figures 2D and 2E). It should be noted that the indoor results cannot perfectly predict its outdoor cooling performance because

Article



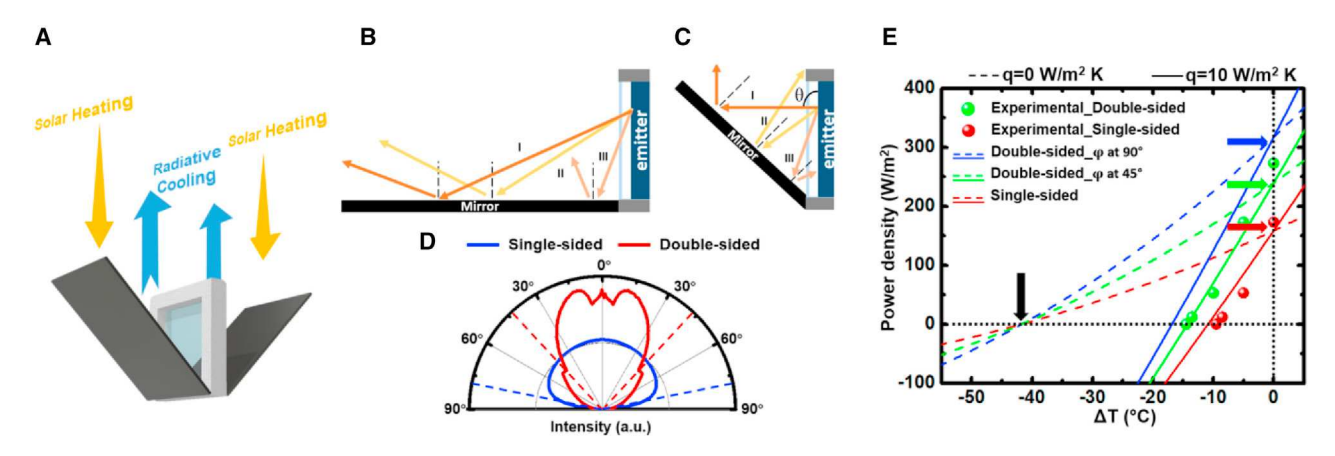


Figure 3. Integrated radiative cooling and solar heating using the same area

(A) Schematic illustration of the vertically aligned double-sided system.

(B and C) Schematic illustration of thermal emission from the emitter when the tilt angle of mirror is at (B) 90° and (C) 45°. Three sets of arrows indicate thermal emission at different angles.

(D) The modeled angular emissive intensity distribution of the single-sided (blue curve) system and V-shaped double-sided system (red curve). The dashed curves show the divergent angles of these two emission patterns at their full widths at half maximum.

(E) Calculated cooling power density (curves) and measured cooling power density (spheres) as a function of temperature difference. Dashed and solid curves represent the case with a thermal transfer coefficient $q = 0 \text{ W/m}^2 \text{ K}$ (dashed curve) and $q = 10 \text{ W/m}^2 \text{ K}$ (solid curve), respectively. The ambient temperature is set to 18°C (for comparison with the indoor experiment shown in Figures 2D and 2E).

the small liquid-nitrogen-based system (with a height of $1\sim2$ m) cannot accurately replicate the transmission feature of the atmospheric window. Therefore, outdoor tests are still necessary, as discussed later. However, considering the uncontrollable weather conditions, no reported outdoor results can actually be compared fairly. In contrast, this indoor setup provides controllable experimental conditions (e.g., humidity, ambient temperature, and wind speed), which allows us to compare different radiative cooling materials and systems.

Because the measured concentrated local cooling power density of 273.3 W/m² is already beyond the blackbody radiation limit for a single surface emitter (Note S1; Figure \$15), it is necessary to clarify the actual merit of the double-sided architecture. Compared with a single-sided system with the same projection area, the double-sided system did not enhance the total cooling power or the cooling power density normalized by the actual surface area of the emitter (i.e., with two surfaces). However, because of the unique vertical configuration, the solar absorption mirrors are spatially separated from the emitter, introducing 2-fold benefits, as illustrated in Figure 3A. The first one is that the two solar absorption mirrors absorb the incident solar energy on them and allow an additional solar heating effect on this radiative cooling system with no extra area requirement (i.e., the heating and cooling channels share the same projection area). The second one is that the local cooling power density of the central thermal emitter is doubled and can result in a lower equilibrium temperature (i.e., 14° C \pm 0.2°C in Figure 2C). This record-high local power density is highly desirable when a lower temperature is required. For instance, the dew point for moisture condensation is dependent on the cooling power density and the actual temperature of the surface (see Figures S4 and S5 and Note S2 for a preliminary experiment to demonstrate this temperature-dependent atmospheric moisture condensation application).

Theoretical analysis

To reveal the superior cooling performance, we analyzed the thermal exchange in a double-sided system under different conditions. When the tilt angle of a mirror, ϕ , is



Cell Reports
Physical Science
Article

90° with infinitely long mirror lengths (i.e., an ideal case), all thermal radiation from both sides of the thermal emitter is coupled to the heat sink, as illustrated in Figure 3B, corresponding to the theoretical upper limit for the proposed system. However, in any realistic situation, the output thermal emission is limited by the mirror length and tilt angle. As illustrated in Figure 3C, when a mirror with finite length is tilted, the thermal emission pattern at distinct emission angles and locations will be different (i.e., cases I, II, and III at different angles). For case I, when the emission angle θ is relatively small, the emitted radiation will be reflected by the mirror and directed to the heat sink. However, as θ increases, part of the emission will be blocked by the top side or bottom side of the emitter, corresponding to cases II and III, respectively. Therefore, the actual output of the thermal emission is reduced. To optimize the thermal emission output, one can tune the tilt angle and manipulate the geometry of the system (for example, using convex mirrors), which is still under investigation. In this work, only the V-shaped structure is considered; i.e., by tuning the tilt angle of the spectrally selective mirror, the thermal emission output can be optimized (see Figure S6 for the normalized emission pattern ε_{pat} with four different tilt angles). As shown in Figure 3D, we modeled the angular distribution of the thermal radiation at a wavelength of 10 μm with a mirror tilt angle of 45°. Compared with the wide thermal radiation pattern from a conventional single-sided system (the blue curve), most of the thermal emission reflected by the V-shaped structure is confined within $\pm 39.8^{\circ}$ (the red curve), which causes a beaming effect of the thermal radiation.

Next, we estimated the theoretical cooling power density and compared it with the observed cooling performance. The net cooling power density (P_{net}) can be calculated as a function of the temperature using Equation 1:

$$P_{\text{net}} = P_{\text{rad}}(T_{\text{dev}}) - P_{\text{amb}}(T_{\text{amb}}) - P_{\text{obj}}(T_{\text{obj}}) - P_{\text{nonrad}}(T_{\text{dev}}, T_{\text{amb}})$$
 (Equation 1)

Here $P_{rad}(T_{dev})$ is the outgoing radiation power from the thermal emitter at a temperature of T_{dev} , $P_{amb}(T_{amb})$ is the incoming radiation power from the ambient environment at a temperature of T_{amb} , $P_{obj}(T_{obj})$ is the thermal radiation transfer between the solar spectrally selective surfaces and emitter surfaces, and $P_{nonrad}(T_{dev}, T_{amb})$ is the non-radiative power transferred to the emitter through convection and conduction. Although the atmosphere is a complex system composed of different layers with gradient temperature, it has been shown that estimation of its radiance can be simplified by assuming a uniform temperature. 47

Using this equation, one can estimate the cooling power density as a function of the temperature difference ΔT (see calculation details in Note S1). As shown in Figure 3E, we plotted the cooling power densities at an ambient temperature of $18^{\circ}C$ for three systems: a double-sided system with a mirror tilt angle of 90° (blue curves), a double-sided system with a mirror tilt angle of 45° (green curves), and a single-sided system (red curves). In particular, the thermal transfer coefficients were set to $q = 0 \text{ W/m}^2 \text{ K}$ (i.e., with perfect thermal insulation; dashed curves) and $q = 10 \text{ W/m}^2 \text{ K}$ (i.e., with parasitic heat loss; solid curves), respectively.

When $\Delta T = 0$ (vertical dashed line), the cooling power densities of the systems with or without parasitic heat loss are the same because there is no conductive or convective heat exchange with the environment. One can see that an ideal double-sided system reaches a local cooling power density of 310.4 W/m² (indicated by the blue arrow), twice as much as that of an ideal single-sided system; i.e.155.2 W/m² (indicated by the red arrow). In contrast, the local cooling power density of the practical double-sided system is 242.3 W/m² (green arrow).

Article



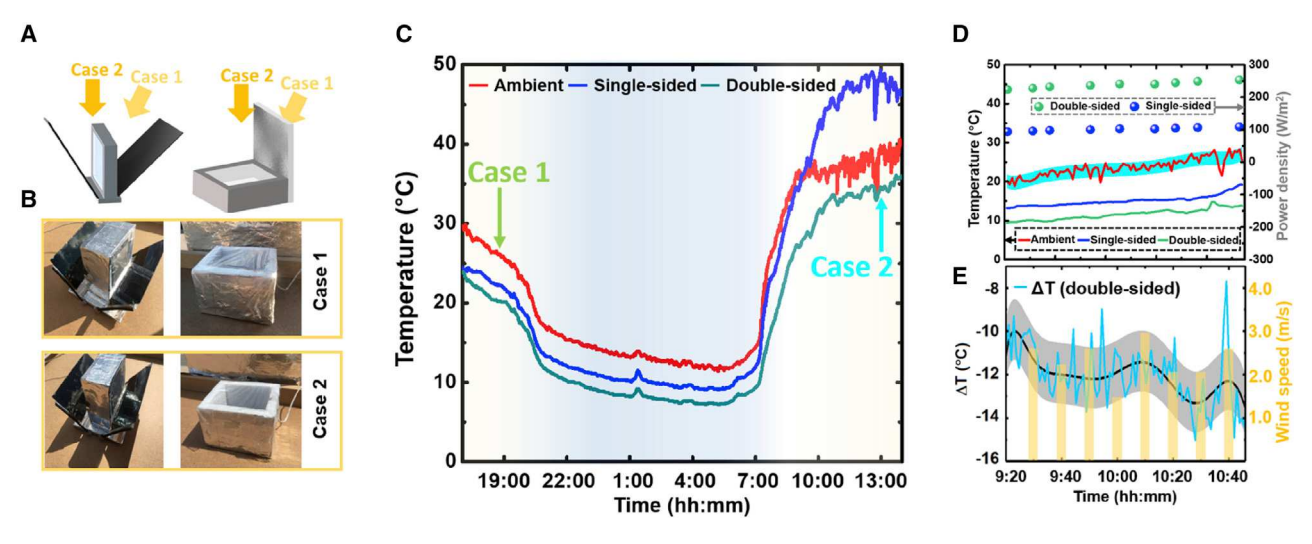


Figure 4. An integrated cooling and heating system with improved daytime sky cooling performance

- (A) Schematic of the daytime radiative cooling tests in Buffalo, NY.
- (B) Photos of the outdoor radiative cooling measurement of case 1 (top panel) and case 2 (bottom panel) with different solar incident angles.
- (C) Measured temperature of the emitter in the double-sided system (green curve) and the single-sided system (blue curve). The ambient temperature is shown by the red curve.
- (D) The best cooling performance was measured on May 21, 2019 in Buffalo, NY. Solid curves indicate the real-time temperature. Spheres indicate the extracted cooling power densities of the double-sided and single-sided systems.
- (E) The temperature difference between the ambient temperature and the emitter in the double-sided system. The yellow bar shows the wind speed at the test location.

Furthermore, the lowest attainable equilibrium temperature of a given system is mainly affected by the spectral features of the thermal emitter and also by the thermal insulation of the system. As indicated by the black arrow at the intersection point of the three dashed curves with zero cooling power density (i.e., the horizontal dashed line in Figure 3E), the equilibrium temperature for these three systems is -23.8°C ($\Delta T = -41.8^{\circ}\text{C}$) with perfect thermal insulation (i.e., $q = 0 \text{ W/m}^2$). However, with parasitic heat loss (e.g., $q = 10 \text{ W/m}^2$), the equilibrium temperature for double-sided systems is lower than that for a single-sided system, agreeing well with our observed experimental results in Figure 2 (shown by green and red spheres). One can see that a double-sided system can realize a lower equilibrium temperature than a single-sided system in the same testing environment, indicating superior performance of the proposed double-sided architecture.

Outdoor tests

To demonstrate the proposed double-sided radiative cooling, we performed outdoor measurements in Buffalo, NY. A single-sided control experiment was performed simultaneously. To further minimize solar absorption, we employed transparent polydimethylsiloxane (PDMS) films as the thermal emitter. As illustrated in Figure 4A, within the double-sided system, the PDMS film was anchored vertically at the center of the polystyrene box, whereas in the single-sided system, the PDMS film was blade coated onto the aluminum back reflector (see the optical absorption spectrum of PDMS in Figure S7). Photographs of the experimental setup are shown in Figure 4B; a highly reflective aluminum board was used to shelter the control system from sunlight (similar to one used previously 14,30), whereas the double-sided emitter system was directly exposed to the sun. We performed a 24-h continuous outdoor test in Buffalo, NY on August 4–5, 2019 (with a humidity of 30% during the day and 95% at night; see more information regarding weather



Cell Reports
Physical Science
Article

conditions in Figure S8). Because of the vertically anchored thermal emitter in the double-sided system, the cooling performance of the system is very different from the single-sided system. As shown by case 1 in Figure 4B, in the single-sided system, the incident sun light was blocked by the shelter but directly illuminated the PDMS film in the double-sided system. As a result, the cooling performance of the double-sided system degraded significantly. Because PDMS is highly transparent in the solar wavelength range, the estimated absorbed solar energy by the PDMS film (\sim 113.95 W/m² under 1 sun illumination) was still much lower than the net radiation power (>200 W/m²). As a result, a sub-ambient cooling effect was still obtained with the double-sided configuration, even without expensive sun-tracking systems. To One can see that at 18:44 in Figure 4C (green arrow), the double-sided system realized a temperature reduction of 6.2°C, whereas Δ T in the single-sided system was 4.2°C.

As the solar input intensity rose steadily over the course of the day/afternoon (Figure 4B, case 2), direct illumination was blocked by the side wall of the polystyrene box in the double-sided system, whereas the planar shelter was unable to block the normal incidence in the single-sided system. This effect could significantly degrade the cooling performance of the device if it were implemented in an area that receives a large amount of harsh sunlight (e.g., Saudi Arabia, as shown in Figure S9). Therefore, the cooling performance of the double-sided emitter system is much greater than that of the single-sided system (see more details in Figure S10 and Note S3). By reviewing the overall performance of the two systems shown in Figure 4C, the double-sided system outperformed the single-sided one in all-day subambient cooling, especially under normal solar incidence (when air-conditioning use is the highest). One can see that at 12:58 (cyan arrow), the temperature in the singlesided system is ~10°C higher than ambient temperature because of the solar heating effect. To counteract this heating effect, many previously published systems utilized white micro/nanomaterials^{8,9,16} or large-scale shelter boards³⁰ that were used to block the sun light. In contrast, the double-sided system remained \sim 4.5°C lower than ambient temperature at this moment. Remarkably, the peak temperature of the two solar absorption wings was ~55-60°C, providing a solar-driven thermal component for heating applications (e.g., solar water heating). With this architecture, these two wings realized solar heating and radiative cooling using the same projection area, representing an integrated concentrated cooling and solar heating system with no need of extra spaces.

Finally, as noted previously, radiative cooling performance is heavily dependent on weather conditions. During May-August 2019 and June 2020, we performed over 80 h in total of outdoor experiments on selected sunny days. It was revealed that the overall cooling performance is dependent on outdoor environmental conditions, including incident solar intensity, relative humidity, wind speed, and cloud distribution (see details in Figures S11 and S12). On May 21, 2019 (with a very clear sky and humidity of \sim 17% during the time of the experiment), an even more intriguing result was observed, as shown in Figure 4D. Obvious fluctuations in ambient temperature were observed because of relatively strong gusts of wind. To better reveal the reduced temperature, we plotted the ΔT curve of the double-sided system in Figure 4E. From 9:20 to 11:00, the average temperature reduction of the double-sided emitter system was 12.0°C ± 1.2°C. During this period, the average temperature of the solar absorption plate was \sim 54°C. By considering its spectral feature, shown in Figure 1D, the thermal load from these two solar absorption plates is \sim 44.2 W/m² (i.e., P_{obj} in Equation 1; see Figure S13 for more details). Therefore, the estimated cooling power density of our double-sided system

Article



is 236.6 \pm 11.8 W/m² (green spheres in Figure 4D; see more details in Note S4). This is a record-high temperature reduction for this simple system with no special thermal insulation. ^{16,30} In contrast, the shaded single-sided system only realized a temperature reduction of 8.5°C \pm 1.5°C, corresponding to a cooling power density of 100.1 \pm 7.3 W/m² (blue spheres in Figure 4D). It should be noted that the outdoor cooling performance is heavily dependent on the actual environmental conditions (e.g., wind speed and relative humidity, some of which have large fluctuations). In our calculation, an approximate parameter of the non-radiative thermal transfer coefficient q was employed (q = 10 W/m² K), similar to Bhatia et al. ¹⁵ (q = 9.6 W/m² K), Kou et al. ²¹ (q = 10 W/m² K), and Rephaeli et al. ³⁴ (q = 6–12 W/M² K).

In conclusion, we developed a double-sided architecture for concentrated radiative cooling and solar heating in a single system. The thermal radiation from both sides of a vertically aligned emitter was coupled to the heat sink to realize a record-high local cooling power density of 273.3 W/m² in a laboratory environment. Under standard atmospheric pressure, we demonstrated a record temperature reduction of $14^{\circ}C$ + 0.2° C in a laboratory environment and 12.0° C \pm 1.2° C in an outdoor test. Further improvement will be possible using an optimized system configuration or employing materials with better spectral selectivity (e.g., the materials reported by Wang et al.⁴⁶ with a solar absorption of 0.95 and thermal emission of 0.075). Moreover, in recently reported studies of radiative cooling, solar input and its heating effect were always undesired within the cooling system (i.e., scattered or reflected). 23,48-50 To utilize this formerly wasted energy, the solar absorption plate allows solar heating and radiative cooling (on the central emitter) to occur within the same system. This hybrid system can contribute simultaneously to a reduction in cooling and heating costs of existing heating, ventilation, and air conditioning utilities^{51–54} and can be integrated with future thermoelectric generator systems to produce more power through the Seebeck effect. 38,55.

EXPERIMENTAL PROCEDURES

Resource availability

Lead contact

Further information and requests for resources and reagents should be directed to and will be fulfilled by the lead contact, Qiaoqiang Gan (qqgan@buffalo.edu).

Materials availability

This study did not generate new unique reagents.

Data and code availability

The published article includes all necessary data required for evaluating the main findings of this study. Any additional data related to this study are available from the lead contact upon request.

Fabrication and characterization of the cermet-based solar spectrally selective film

The cermet-based solar absorption film was fabricated in a Lesker sputtering coater system by simultaneously co-sputtering Ag and SiO_2 . A glass substrate was cleaned using a standard wafer cleaning procedure. We started deposition with a 30-nm-thick silver layer (layer 1), followed by 8 layers of Ag/SiO_2 nanocomposites with a gradually changing silver-to-silica ratio (layers 2–9). Finally, a thin silica layer (~30 nm) was deposited as the top layer (layer 10). This stacked structure formed a graded nanocomposite metamaterial with a gradually changing refractive index,



Cell Reports
Physical Science
Article

resulting in broadband absorption from 300 nm to 2 μm . On the other hand, its reflection in the mid-infrared domain is high (Figure 1D).

Laboratory radiative cooling measurements

The thermally insulated container for radiative cooling tests consists of polystyrene foam covered by a layer of aluminized Mylar, as illustrated in Figure S14. For the double-sided system, the dimension of the frame is 6 \times 6 cm. The thickness of the side wall of the frame is 4 cm. The thermal emitter is anchored in the center of the frame, as shown in Figure S14, left panel. Two transparent polyethylene films are used to seal the aperture on both sides. For the single-sided system, the polystyrene frame has one aperture only, as shown in Figure S14, right panel. With these designs, the thermal conductivities of the polystyrene foam and the air gap is 0.033 W/(m·K) and 0.026 W/(m·K), respectively, at 25°C.

In the indoor experiment, a black aluminum sheet was immersed in liquid nitrogen to serve as the heat sink. Its absorption/emission spectrum is shown in Figure S3. The thermal emitter was placed $\sim\!1.6$ m above the heat sink to prevent thermal conduction/convection from the liquid nitrogen. An aluminum plate waveguide was employed to connect the heat sink with the thermal emitter. A K-type probe was mounted on the tested system to measure ambient temperature.

The cooling power densities for both setups were measured, as shown in Figures 2D and 2E, following the procedure reported by Bhatia et al. 15 . Black aluminum sheets were employed as the thermal emitter. The cooling power was determined by measuring the electrical input power of the polyimide flexible heater (Omega, KHLV series, $14.5~\Omega/0.0025~m^2$). In the single-sided system, the heater was attached to the back of the black aluminum. In the double-sided system, the heater was sandwiched between two black aluminum sheets.

Optical measurements

The reflection spectrum of the solar spectrally selective film was measured using a Vis-NIR-MIR Fourier transform infrared spectrometer (Vertex 70, Bruker) with an angle module (Bruker A513 variable-angle reflection accessory).

SUPPLEMENTAL INFORMATION

Supplemental Information can be found online at https://doi.org/10.1016/j.xcrp. 2021.100338.

ACKNOWLEDGMENTS

This work was supported by the National Science Foundation (CBET-1932968 and 1932843).

AUTHOR CONTRIBUTIONS

Supervision and conceptualization, Q.G.; investigation, L.Z., H.S., N.Z., J.R., and M.S.; writing – original draft, L.Z., H.S., J.R., M.S., H.Z., Z.Y., B.S.O., and Q.G.; writing – review & editing, L.Z., J.R., and Q.G.; resources, B.S.O., Z.Y., and Q.G.

DECLARATION OF INTERESTS

L.Z., H.S., Z.Y., and Q.G. are named as inventors on a provisional patent application pertaining to this work (US patent 62/844,120). Q.G. and Z.Y. have founded a

Article



company, Sunny Clean Water LLC, seeking to commercialize the results reported in this paper.

Received: June 29, 2020 Revised: December 7, 2020 Accepted: January 14, 2021 Published: February 8, 2021

REFERENCES

- Mat, S. (2016). Cooling the buildings past, present and future. Energy Build. 128, 617–638.
- U.S. Energy Information Administration (2016). Transportation sector energy consumption. International Energy Outlook 2016 (U.S. Department of Energy), pp. 127–138.
- 3. Chu, S., and Majumdar, A. (2012). Opportunities and challenges for a sustainable energy future. Nature 488, 294–303.
- Raman, A.P., Anoma, M.A., Zhu, L., Rephaeli, E., and Fan, S. (2014). Passive radiative cooling below ambient air temperature under direct sunlight. Nature 515, 540–544.
- Shi, N.N., Tsai, C.C., Camino, F., Bernard, G.D., Yu, N., and Wehner, R. (2015). Thermal physiology. Keeping cool: Enhanced optical reflection and radiative heat dissipation in Saharan silver ants. Science 349, 298–301.
- Zhou, M., Song, H., Xu, X., Shahsafi, A., Xia, Z., Ma, Z., Kats, M., Zhu, J., Ooi, B.S., Gan, Q., et al. (2018). Accelerating vapor condensation with daytime radiative cooling. arXiv, arXiv:1804.10736. https://arxiv.org/abs/1804.
- Zhai, Y., Ma, Y., David, S.N., Zhao, D., Lou, R., Tan, G., Yang, R., and Yin, X. (2017). Scalablemanufactured randomized glass-polymer hybrid metamaterial for daytime radiative cooling. Science 355, 1062–1066.
- 8. Hsu, P.C., Song, A.Y., Catrysse, P.B., Liu, C., Peng, Y., Xie, J., Fan, S., and Cui, Y. (2016). Radiative human body cooling by nanoporous polyethylene textile. Science 353, 1019–1023.
- 9. Hsu, P.C., Liu, C., Song, A.Y., Zhang, Z., Peng, Y., Xie, J., Liu, K., Wu, C.L., Catrysse, P.B., Cai, L., et al. (2017). A dual-mode textile for human body radiative heating and cooling. Sci. Adv. 3, e1700895.
- Mandal, J., Fu, Y., Overvig, A.C., Jia, M., Sun, K., Shi, N.N., Zhou, H., Xiao, X., Yu, N., and Yang, Y. (2018). Hierarchically porous polymer coatings for highly efficient passive daytime radiative cooling. Science 362, 315–319.
- Li, T., Zhai, Y., He, S., Gan, W., Wei, Z., Heidarinejad, M., Dalgo, D., Mi, R., Zhao, X., Song, J., et al. (2019). A radiative cooling structural material. Science 364, 760–763.
- Peng, Y., Chen, J., Song, A.Y., Catrysse, P.B., Hsu, P.C., Cai, L., Liu, B., Zhu, Y., Zhou, G., Wu, D.S., et al. (2018). Nanoporous polyethylene microfibres for large-scale radiative cooling fabric. Nat. Sustain. 1, 105–112.
- Zhang, X.A., Yu, S., Xu, B., Li, M., Peng, Z., Wang, Y., Deng, S., Wu, X., Wu, Z., Ouyang, M., and Wang, Y. (2019). Dynamic gating of

- infrared radiation in a textile. Science 363, 619–623.
- Zhou, L., Song, H., Liang, J., Singer, M., Zhou, M., Stegenburgs, E., Zhang, N., Xu, C., Ng, T., Yu, Z., et al. (2019). A polydimethylsiloxanecoated metal structure for all-day radiative cooling. Nat. Sustain. 2, 718–724.
- Bhatia, B., Leroy, A., Shen, Y., Zhao, L., Gianello, M., Li, D., Gu, T., Hu, J., Soljačić, M., and Wang, E.N. (2018). Passive directional subambient daytime radiative cooling. Nat. Commun. 9, 5001.
- Leroy, A., Bhatia, B., Kelsall, C.C., Castillejo-Cuberos, A., Di Capua H, M., Zhao, L., Zhang, L., Guzman, A.M., and Wang, E.N. (2019). Highperformance subambient radiative cooling enabled by optically selective and thermally insulating polyethylene aerogel. Sci. Adv. 5, eaat9480.
- Hossain, M.M., and Gu, M. (2016). Radiative Cooling: Principles, progress, and potentials. Adv. Sci. (Weinh.) 3, 1500360.
- 18. Fan, S. (2017). Thermal photonics and energy applications. Joule 1, 264–273.
- Sun, X., Sun, Y., Zhou, Z., Alam, M., and Bermel, P. (2017). Radiative sky cooling: fundamental physics, materials, structures, and applications. Nanophotonics 6, 997–1015.
- Zhao, B., Hu, M., Ao, X., Chen, N., and Pei, G. (2019). Radiative cooling: A review of fundamentals, materials, applications, and prospects. Appl. Energy 236, 489–513.
- Kou, J.I., Jurado, Z., Chen, Z., Fan, S., and Minnich, A.J. (2017). Daytime radiative cooling using near-black infrared emitters. ACS Photonics 4, 626–630.
- Zhu, R., Hu, D., Chen, Z., Xu, X., Zou, Y., Wang, L., and Gu, Y. (2020). Plasmon-enhanced infrared emission approaching the theoretical limit of radiative cooling ability. Nano Lett. 20, 6974–6980.
- Chen, Z., Zhu, L., Li, W., and Fan, S. (2019). Simultaneously and synergistically harvest energy from the sun and outer space. Joule 3, 101–110.
- Granqvist, C.G., and Hjortsberg, A. (1980). Surfaces for radiative cooling: silicon monoxide films on aluminum. Appl. Phys. Lett. 36, 139–141.
- Granqvist, C.G. (1981). Radiative heating and cooling with spectrally selective surfaces. Appl. Opt. 20, 2606–2615.
- 26. Granqvist, C.G., Hjortsberg, A., and Eriksson, T.S. (1982). Radiative cooling to low

- temperatures with selectivity IR-emitting surfaces. Thin Solid Films 90, 187–190.
- Catalanotti, S., Cuomo, V., Piro, G., Ruggi, D., Silverstrini, V., and Troise, G. (1975). The radiative cooling of selective surfaces. Sol. Energy 17, 83–89.
- 28. Head, A.K. (1962). US patent 3043112A, filed January 12, 1960, and published July 10, 1962.
- Trombe, F. (1967). Perspectives sur l'utilisation des rayonnements solaires et terrestres dans certaines re'gions du monde. Revue Générale Thermique 6, 1285–1314.
- Chen, Z., Zhu, L., Raman, A., and Fan, S. (2016). Radiative cooling to deep sub-freezing temperatures through a 24-h day-night cycle. Nat. Commun. 7, 13729.
- 31. Li, W., Shi, Y., Chen, Z., and Fan, S. (2018). Photonic thermal management of coloured objects. Nat. Commun. 9, 4240.
- 32. Gentle, A.R., and Smith, G.B. (2015). A Subambient open roof surface under the mid-summer sun. Adv. Sci. (Weinh.) 2, 1500119.
- Atiganyanun, S., Plumley, J.B., Han, S.J., Hsu, K., Cytrynbaum, J., Peng, T.L., Han, S.M., and Han, S.E. (2018). Effective radiative cooling by paint-format microsphere-based photonic random media. ACS Photonics 5, 1181–1187.
- Rephaeli, E., Raman, A., and Fan, S. (2013). Ultrabroadband photonic structures to achieve high-performance daytime radiative cooling. Nano Lett. 13, 1457–1461.
- Goldstein, E.A., Raman, A.P., and Fan, S. (2017). Sub-ambient non-evaporative fluid cooling with the sky. Nat. Energy 2, 17143.
- Smith, G.B. (2009). Amplified radiative cooling via optimised combinations of aperture geometry and spectral emittance profiles of surfaces and the atmosphere. Sol. Energy Mater. Sol. Cells 93, 1696–1701.
- 37. Tso, C.Y., Chan, K.C., and Chao, C.Y.H. (2017). A field investigation of passive radiative cooling under Hong Kong's climate. Renew. Energy 106, 52–61.
- Raman, A.P., Li, W., and Fan, S. (2019).
 Generating light from darkness. Joule 3, 2679– 2686
- Cao, F., McEnaney, K., Chen, G., and Ren, Z. (2014). A review of cermet-based spectrally selective solar absorbers. Energy Environ. Sci. 7, 1615–1627.
- Granqvist, C.G., and Hunderi, O. (1978).
 Optical properties of Ag-SiO2 Cermet films: A comparison of effective-medium theories.
 Phys. Rev. B Condens. Matter 18, 2897–2906.



Cell Reports Physical Science Article

- Biener, J., Nyce, G.W., Hodge, A.M., Biener, M.M., Hamza, A.V., and Maier, S.A. (2008). Nanoporous Plasmonic Metamaterials. Adv. Mater. 20, 1211–1217.
- Zhang, N., Liu, K., Song, H., Liu, Z., Ji, D., Zeng, X., Jiang, S., and Gan, Q. (2014). Refractive index engineering of metal-dielectric nanocomposite thin films for optical super absorber. Appl. Phys. Lett. 104, 203112.
- Song, H., Guo, L., Liu, Z., Liu, K., Zeng, X., Ji, D., Zhang, N., Hu, H., Jiang, S., and Gan, Q. (2014). Nanocavity enhancement for ultra-thin film optical absorber. Adv. Mater. 26, 2737–2743, 2617.
- Liu, K., Zeng, X., Jiang, S., Ji, D., Song, H., Zhang, N., and Gan, Q. (2014). A large-scale lithography-free metasurface with spectrally tunable super absorption. Nanoscale 6, 5599–
- Kennedy, C.E. (2002). Review of Mid- to High-Temperature Solar Selective Absorber Material. July 2002, NREL/TP-520-31267. https://www.nrel.gov/docs/fy02osti/31267. pdf.

- Wang, J., Wei, B., Wei, Q., and Li, D. (2011). Optical property and thermal stability of Mo/ Mo–SiO2/SiO2 solar-selective coating prepared by magnetron sputtering. Phys. Status Solidi 208, 664–667.
- Li, M., and Coimbra, C.F.M. (2019). On the effective spectral emissivity of clear skies and the radiative cooling potential of selectively designed materials. Int. J. Heat Mass Transf. 135, 1053–1062.
- Byrnes, S.J., Blanchard, R., and Capasso, F. (2014). Harvesting renewable energy from Earth's mid-infrared emissions. Proc. Natl. Acad. Sci. USA 111, 3927–3932.
- Buddhiraju, S., Santhanam, P., and Fan, S. (2018). Thermodynamic limits of energy harvesting from outgoing thermal radiation. Proc. Natl. Acad. Sci. USA 115, E3609–E3615.
- Zhu, L., Raman, A.P., and Fan, S. (2015). Radiative cooling of solar absorbers using a visibly transparent photonic crystal thermal blackbody. Proc. Natl. Acad. Sci. USA 112, 12282–12287.

- Reyna, J.L., and Chester, M.V. (2017). Energy efficiency to reduce residential electricity and natural gas use under climate change. Nat. Commun. 8, 14916.
- Laine, H.S., Salpakari, J., Looney, E.E., Savin, H., Peters, I.M., and Buonassisi, T. (2019). Meeting global cooling demand with photovoltaics during the 21st century. Energy Environ. Sci. 12, 2706–2716.
- 53. She, X., Cong, L., Nie, B., Leng, G., Peng, H., Chen, Y., Zhang, X., Wen, T., Yang, H., and Luo, Y. (2018). Energy-efficient and -economic technologies for air conditioning with vapor compression refrigeration: A comprehensive review. Appl. Energy 232, 157–186.
- Li, M., Peterson, H.B., and Coimbra, C.F.M. (2019). Radiative cooling resource maps for the contiguous United States. J. Renew. Sustain. Energy 11, 036501.
- 55. Li, W., Buddhiraju, S., and Fan, S. (2020). Thermodynamic limits for simultaneous energy harvesting from the hot sun and cold outer space. Light Sci. Appl. 9, 68.